Chinese Journal of Aeronautics, (2014),27(5): 1171–1179

Chinese Society of Aeronautics and Astronautics
& Beihang University

Chinese Journal of Aeronautics

cja@buaa.edu.cn
www.sciencedirect.com

Changing law of launching pitching angular velocity of rotating missile

Liu Guang [a,b,*], Xu Bin [a,b], Jiao Xiaojuan [a], Zhen Tiesheng [a]

[a] Department of Mechanics and Engineering Science, Fudan University, Shanghai 200433, China
[b] Shanghai Electro-Mechanical Engineering Institute, Shanghai 201109, China

Received 22 March 2013; revised 2 April 2014; accepted 1 August 2014
Available online 28 September 2014

KEYWORDS

LPAV;
MFBD;
Modeling;
Rotating missile;
Simulation;
Virtual prototyping

Abstract In order to provide accurate launching pitching angular velocity (LPAV) for the exterior trajectory optimization design, multi-flexible body dynamics (MFBD) technology is presented to study the changing law of LPAV of the rotating missile based on spiral guideway. An MFBD virtual prototype model of the rotating missile launching system is built using multi-body dynamics modeling technology based on the built flexible body models of key components and the special force model. The built model is verified with the frequency spectrum analysis. With the flexible body contact theory and nonlinear theory of MFBD technology, the research is conducted on the influence of a series of factors on LPAV, such as launching angle change, clearance between launching canister and missile, thrust change, thrust eccentricity and mass eccentricity, etc. Through this research, some useful values of the key design parameters which are difficult to be measured in physical tests are obtained. Finally, a simplified mathematical model of the changing law of LPAV is presented through fitting virtual test results using the linear regression method and verified by physical flight tests. The research results have important significance for the exterior trajectory optimization design.

1. Introduction

A rotating missile is a terminal defense weapon with quick reactions, high launching efficiency and simple structure, etc., the main function of which is to intercept and attack sea-skimming flight anti-ship missiles and high-speed aircrafts. The missile has important practical significance to the coastal defense of the South China Sea. When the missile is launched, the empennage seat is used as a support and contact with the side of spiral guideway in the launching canister so that the missile moves along with the spiral guideway to achieve the rotation movement of the missile launching. In the process of launching the rotating missile, its launching pitching angular velocity (LPAV) must be some dispersed and difficult to be determined due to a variety of influencing factors such as launching angle change, clearance between launching canister and missile, thrust change, thrust eccentricity and mass eccentricity, etc.

* Corresponding author at: Department of Mechanics and Engineering Science, Fudan University, Shanghai 200433, China. Tel.: +86 21 24185555.
E-mail addresses: liuguang_nwpu@163.com (G. Liu), Zhengts@fudan.edu.cn (T. Zhen).

Peer review under responsibility of Editorial Committee of CJA.

Production and hosting by Elsevier

http://dx.doi.org/10.1016/j.cja.2014.09.004

LPAV is an important initial parameter in the exterior trajectory design.[1] The past flight test results prove that the improper parameter value would result in large deviation between theoretical and flight test trajectories, and lead to flight test failure eventually. Therefore, the changing law of LPAV has some significance for the exterior trajectory optimization design. In order to find out the changing law of LPAV of the rotating missile and provide an accurate initial parameter for the exterior trajectory design, it is of necessity to make dynamic modeling and simulation of the rotating missile launching process.[2–4] The traditional mathematic modeling method of launching dynamics is very tedious and the built model is largely simplified, therefore it cannot accurately consider the complex collision between the launching canister and the missile, and even the elastic vibration, large deformation and nonlinear vibration of the missile, the launching canister and the rack.[5–7] Multi-rigid body launching dynamics modeling and simulation technology provides an effective solution to the rotating missile development problems, which considers only the complex collision between the launching canister and the missile but the vibration and deformation of the missile body, the launching canister and the rack.[8,9] The past flight test results prove that LPAV from multi-rigid body launching dynamics simulation cannot satisfy the exterior trajectory design requirement. Rigid-flexible coupling launching dynamics modeling and simulation technology based on the Craig-Bampton modal synthesis method considers only the linear elastic deformation of parts, but the collision between flexible bodies, and not even the larger deformation and nonlinear analysis.[10–14] Therefore, multi-flexible body dynamics (MFBD) modeling and simulation technology is presented to solve the above problems.[15] MFBD technology enables designers to simulate the mechanical environment more really at rotating missile launching.

Therefore, in this paper the rotating missile launching system is taken as an example, and its multi-body dynamics model is built based on the MFBD technology using the modal synthesis method and the nodal method. Based on the built model, the research is conducted on the influence of a series of factors on LPAV such as launching angle change, clearance between launching canister and missile, thrust change, thrust eccentricity and mass eccentricity, etc., using the flexible body contact theory and the nonlinear theory of MFBD technology and we obtain some significant values of the key design parameters which are difficult to be measured in physical tests. Finally, a simplified mathematical model of the changing law of LPAV is presented through fitting the virtual test results by means of the linear regression method and is verified by physical flight tests. The research results have important significance for the exterior trajectory optimization design.

2. Components of launching system and analysis of launching process

The spiral guideway launching system is divided into launcher and missile according to its structural feature. The launcher is composed of U-bracket, launching rack and launching canister. The missile is composed of body, bourrelet, folding rudder and folding empennage. Its topological structure is shown in Fig. 1.

In the launching process, the movement relations of the various components are as follows: after the ignition of the engine, the missile is locked by the lock device and does not move. When the thrust increases to a critical value, the lock device unlocks. The side of empennage seat moves along with the spiral guideway in the launching canister in the role of the bourrelet to achieve the rotation movement of the missile launching. The front and back bourrelet detach the spiral guideway respectively, and also the folding rudder and the folding empennage automatically spread, position and lock respectively.

3. MFBD model of launching system

On the basis of building the finite element model of U-bracket, launching rack, launching canister and missile, according to the topological structure of launching system, in the RecurDyn's simulation environment, the MFBD virtual prototype physical mode of the spiral guideway launching system of the rotating missile is built as Fig. 2.

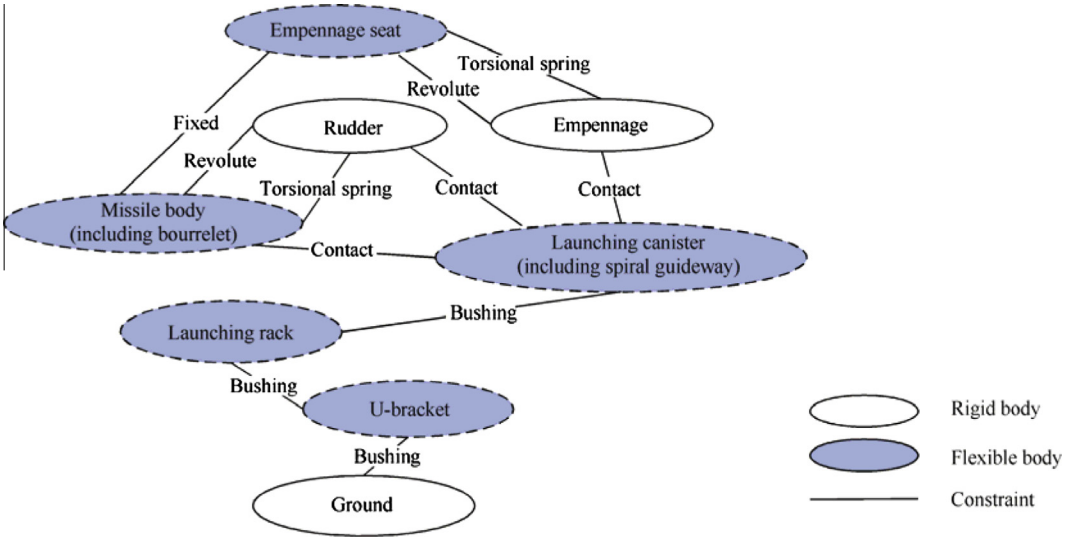

Fig. 1 Topological structure of launching system.

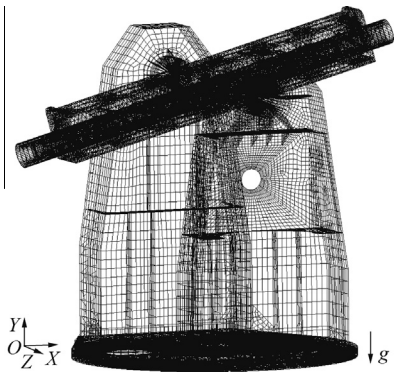

Fig. 2 MFBD model of launching system.

3.1. Flexible body

In this launching system, U-bracket and launching rack are reusable products, and there is only hinge relationship between other parts. Their elastic deformation has a certain influence on the attitude of the missile launching, and the elastic deformation of U-bracket and launching rack is very small in the process of missile launching, so the flexible body models of U-bracket and launching rack are built using the Craig-Bampton modal synthesis method.[10–14] The Craig-Bampton modal synthesis method is a particularly effective method to reduce degrees of freedom, whose basic idea is that a flexible body is given a set of modes and its deformation can be expressed using a linear combination of modal vectors and modal coordinates.[16]

Using the Craig-Bampton modal synthesis method, the building process of flexible body models of U-bracket and launching rack is: Firstly, through components grid discretization and a series of relevant definitions in the finite element modeling software Patran, the finite element model input files (∗·bdf) are generated. Secondly, in the ∗·bdf file add the RecurDyn flexbody interface (RFI) file control command: MBDEXPORT RECURDYN FLEXBODY = YES, FLEXONLY = YES, OUTGSTRS = YES, OUTGSTRN = YES. Thirdly, the modified ∗·bdf files are submitted to the finite element solver NX Nastran for mode calculation to automatically generate the required RFI modal neutral file. Finally, the RFI modal neutral files are read to build flexible body models of U-bracket and launching rack model via R/Flex interface in RecurDyn. The modal parameters of U-bracket and launching rack are shown in Table 1.

In this launching system, the missile and the launching canister are not reusable products, and their structures are slender and thin-walled, so they easily bend in the process of work. In the launching process, there exists complex collision between the spiral guideway and several cabins of the rotating missile body. At the point of contact, there exists local contact nonlinearity and material nonlinearity. In order to accurately calculate the collision force and non-linear deformation and evaluate LPAV, MFBD technology is adopted to build the flexible body models of the launching canister and the missile body. MFBD technology expands the Craig-Bampton modal synthesis method with the nodal method and defines a flexible body by using industry-standard file to read finite element meshes.[17–21] It truly simulates contact nonlinearity and material nonlinearity between the spiral guideway of the launching canister and the body of the rotating missile using the nodal method.

Table 1 Modal parameters of U-bracket and launching rack.

Order	Frequency of U-bracket (Hz)	Frequency of launching rack (Hz)
1	23.29	153.46
2	42.87	164.72
3	43.18	214.18
4	60.88	249.67
5	133.59	336.31
6	142.38	397.06
7	143.07	477.88
8	148.88	482.30
9	171.95	495.52
10	176.49	510.18
11	195.31	535.73
12	204.55	607.80
13	220.45	744.78
14	233.76	803.04
15	236.72	958.61

Using the nodal method, the building process of flexible body models of the missile and the launching canister is: through components grid discretization and a series of relevant definitions in the finite element modeling software Patran, the finite element model input files (∗·bdf) are generated, which is directly read to build flexible body models of the missile and the launching canister via F/Flex interface in RecurDyn. The flexible body model of the launching canister consists of 45408 nodes and 25742 elements and element type is Solid8 (CHEXA). The flexible body model of the missile consists of 11522 nodes and 10451 elements, and element type is Shell4 (QUAD4) and Mass (CONM2).

3.2. Special force

3.2.1. Contact force

Using a nonlinear parallel spring and damper, the contact force is simulated between the missile and the spiral guideway, as well as between the empennage seat and the spiral guideway in the model. The Coulomb friction effect is considered in the contact process and the contact force calculation formula can be expressed as[15]

$$\boldsymbol{f} = k\boldsymbol{d}^{m_1} + c\frac{\dot{\boldsymbol{d}}}{|\dot{\boldsymbol{d}}|}|\dot{\boldsymbol{d}}|^{m_2}\boldsymbol{d}^{m_3} \tag{1}$$

where k and c are the spring and damping coefficients which are determined by an experimental method respectively. $\boldsymbol{d}$ is penetration depth and the $\dot{\boldsymbol{d}}$ is time differentiation of $\boldsymbol{d}$. The exponents m_1 and m_2 generate a non-linear contact force and the exponent m_3 yields an indentation damping effect. The values of contact parameters are shown in Table 2.

3.2.2. Aerodynamic force

In the launching process, the angle of attack of the rotating missile is zero, and the aerodynamic force cannot be expressed using lift, drag and lateral force, so the aerodynamic load of the missile is simplified as follows. Ignore the random disturbance of wind and only consider the horizontal steady wind[22]; ignore the change of the missile windward area and the

Table 2 Values of contact parameter.

Contact parameter	Value
k (N/m)	3.5×10^{7}
c (N·s/m)	2.8×10^{4}
$\boldsymbol{d}_{\max}$ (m)	1.0×10^{-4}
m_1	2.0
m_2	1.5
m_3	2.0

uniform aerodynamic force is simplified as the concentration perturbation force, is act on the pressure center of the missile and is perpendicular to the longitudinal axis of the missile; the formula is

$$\boldsymbol{F}_{\mathrm{a}} = C_{\mathrm{n}}(\boldsymbol{v}_{\mathrm{m}}^2 + \boldsymbol{v}_{\mathrm{w}}^2)S/2 \tag{2}$$

where the specific numerical value of wind load coefficient C_{n} and wind load reference area S can be obtained by wind tunnel experiments, $\boldsymbol{v}_{\mathrm{w}}$ is the velocity of steady wind, and $\boldsymbol{v}_{\mathrm{m}}$ is the transverse velocity of missile. Because $\boldsymbol{F}_{\mathrm{a}}$ is a function of $\boldsymbol{v}_{\mathrm{m}}$, $\boldsymbol{F}_{\mathrm{a}}$ is corrected in real time by compiling a feedback control function.

3.2.3. Thrust

The engine thrust is simulated using unidirectional force, of which direction changes with the missile motion attitude, which can be realized by interpolation function AKISPL. AKISPL function can be expressed as

$$\mathrm{AKISPL}(t, 0, \mathrm{spline\_}n, 0) \tag{3}$$

where t is simulation analysis time, spline_n is engine thrust curve. Multiple engine performance curves can set according to needs; the influence of different engine thrust on the performance of the launching system is validated in the simulation.

3.2.4. Flexible connection force

To more accurately simulate parts' joint relations, Bushing method is adopted to connect U-bracket, the ground and launching rack, as well as launching rack and canister. Bushing connects parts with 3-direction translational and rotational force at the connecting point.[15] Bushing force model is shown in Eq. (4) and its parameters are gained per modal test parameter identification.[23,24]

$$\begin{bmatrix}\boldsymbol{F}_{ax}\\ \boldsymbol{F}_{ay}\\ \boldsymbol{F}_{az}\\ \boldsymbol{T}_{ax}\\ \boldsymbol{T}_{ay}\\ \boldsymbol{T}_{az}\end{bmatrix} = -\begin{bmatrix}K_{11}&0&0&0&0&0\\ 0&K_{22}&0&0&0&0\\ 0&0&K_{33}&0&0&0\\ 0&0&0&K_{44}&0&0\\ 0&0&0&0&K_{55}&0\\ 0&0&0&0&0&K_{66}\end{bmatrix}\begin{bmatrix}\boldsymbol{L}_{\mathrm{ab1}}^{k_1}\\ \boldsymbol{L}_{\mathrm{ab2}}^{k_2}\\ \boldsymbol{L}_{\mathrm{ab3}}^{k_3}\\ \boldsymbol{\theta}_{\mathrm{ab1}}^{l_1}\\ \boldsymbol{\theta}_{\mathrm{ab2}}^{l_2}\\ \boldsymbol{\theta}_{\mathrm{ab3}}^{l_3}\end{bmatrix} - \begin{bmatrix}C_{11}&0&0&0&0&0\\ 0&C_{22}&0&0&0&0\\ 0&0&C_{33}&0&0&0\\ 0&0&0&C_{44}&0&0\\ 0&0&0&0&C_{55}&0\\ 0&0&0&0&0&C_{66}\end{bmatrix}\begin{bmatrix}\boldsymbol{v}_{\mathrm{ab1}}^{m_1}\\ \boldsymbol{v}_{\mathrm{ab2}}^{m_2}\\ \boldsymbol{v}_{\mathrm{ab3}}^{m_3}\\ \boldsymbol{\omega}_{\mathrm{ab1}}^{n_1}\\ \boldsymbol{\omega}_{\mathrm{ab2}}^{n_2}\\ \boldsymbol{\omega}_{\mathrm{ab3}}^{n_3}\end{bmatrix} + \begin{bmatrix}\boldsymbol{F}_1\\ \boldsymbol{F}_2\\ \boldsymbol{F}_3\\ \boldsymbol{T}_1\\ \boldsymbol{T}_2\\ \boldsymbol{T}_3\end{bmatrix} \tag{4}$$

Table 3 Values of bushing parameter.

Bushing parameter	Value
K_{ii} (i = 1, 2, 3) (N/m)	$(3.4\text{–}8.0)\times10^{7}$
K_{ii} (i = 4, 5, 6)/(N·m/(°))	$(4.8\text{–}8.0)\times10^{5}$
C_{ii} (i = 1, 2, 3) (N·s/m)	$(3.1\text{–}5.0)\times10^{3}$
C_{ii} (i = 4, 5, 6)/(N·m·s/(°))	$(1.3\text{–}5.0)\times10^{3}$
k_i (i = 1, 2, 3)	1.2
l_i (i = 1, 2, 3)	1.2
m_i (i = 1, 2, 3)	1.2
n_i (i = 1, 2, 3)	1.2

where K_{ii} (i = 1, 2, 3, 4, 5, 6) is the stiffness, and C_{ii} (i = 1, 2, 3, 4, 5, 6) is the damping. $\boldsymbol{L}_{\mathrm{ab}i}$ and $\boldsymbol{\theta}_{\mathrm{ab}i}$ (i = 1, 2, 3) are the translational and rotational displacements of the action marker with respect to the base marker. $\boldsymbol{v}_{\mathrm{ab}i}$ and $\boldsymbol{\omega}_{\mathrm{ab}i}$ (i = 1, 2, 3) are the translational and rotational velocities of the action marker with respect to the base marker. $\boldsymbol{F}_i$ and $\boldsymbol{T}_i$ (i = 1, 2, 3) are the constant preloads applied to the action marker. k_i, l_i, m_i and n_i (i = 1, 2, 3) are exponents. The values of bushing parameters are shown in Table 3.

3.2.5. Torsion spring

The folding rudder and folding empennage are movable relative to the missile body. The folding locking mechanism of the rudder and empennage are very complex; therefore, the simplified folding rudder and folding empennage models are established using a special way. The torsion spring is simulated by a torsional spring-damping, and the expression is

$$\boldsymbol{T} = -K_T(\boldsymbol{\theta} - \boldsymbol{\theta}_0) - C_T\dot{\boldsymbol{\theta}} + \boldsymbol{T}_0 \tag{5}$$

where $\boldsymbol{\theta}$ is the torsional angle, $\boldsymbol{\theta}_0$ is the pre-torsional angle, K_T and C_T are the torsional stiffness and damping respectively, and $\boldsymbol{T}_0$ is the pre-torque.

Before launching missile, these rotating parts are turned and pressed into the launching canister. When leaving the launching canister, they are automatically unfolded in the effect of torsion spring, and locked and positioned using a specific locking mechanism. In order to reduce the disturbance to the attitude of the missile at the time of position, the bigger impact force damping is adopted to abate the vibration energy rapidly.

3.3. MFBD equation of launching system

According to the built MFBD virtual prototype physical model of the spiral guideway launch system, based on the variational form of the Newton–Euler equations for a constraint mechanism, the multi-rigid body motion equation of the launching system is built using the principle of virtual work:

$$\boldsymbol{F}^{\mathrm{r}} = \boldsymbol{B}^{\mathrm{T}}(\boldsymbol{M}\ddot{\boldsymbol{r}} + (\boldsymbol{\Phi}_Z^{\mathrm{rr}})^{\mathrm{T}}\boldsymbol{\lambda}^{\mathrm{rr}} + (\boldsymbol{\Phi}_Z^{\mathrm{er}})^{\mathrm{T}}\boldsymbol{\lambda}^{\mathrm{er}} - \boldsymbol{Q}^{\mathrm{r}}) = \boldsymbol{0} \tag{6}$$

Combined with the finite element motion equation of flexible bodies, there is

$$\boldsymbol{F}^{\mathrm{e}} = \boldsymbol{M}^{\mathrm{e}}\ddot{\boldsymbol{q}}^{\mathrm{e}} + (\boldsymbol{\Phi}_{\boldsymbol{q}^{\mathrm{e}}}^{\mathrm{ee}})^{\mathrm{T}}\boldsymbol{\lambda}^{\mathrm{ee}} - \boldsymbol{Q}^{\mathrm{e}} = \boldsymbol{0} \tag{7}$$

Using MFBD technology and relative coordinate system, the equation of the launching system is established:

$$\begin{bmatrix} \dfrac{\partial \boldsymbol{F}^{\mathrm{e}}}{\partial \boldsymbol{q}^{\mathrm{e}}} & \dfrac{\partial \boldsymbol{F}^{\mathrm{e}}}{\partial \boldsymbol{q}^{\mathrm{r}}} & \boldsymbol{0} & (\boldsymbol{\Phi}_{q^{\mathrm{e}}}^{\mathrm{er}})^{\mathrm{T}} \\ \dfrac{\partial \boldsymbol{F}^{\mathrm{r}}}{\partial \boldsymbol{q}^{\mathrm{e}}} & \dfrac{\partial \boldsymbol{F}^{\mathrm{r}}}{\partial \boldsymbol{q}^{\mathrm{r}}} & \boldsymbol{B}^{\mathrm{T}}(\boldsymbol{\Phi}_{z}^{\mathrm{rr}})^{\mathrm{T}} & \boldsymbol{B}^{\mathrm{T}}(\boldsymbol{\Phi}_{z}^{\mathrm{er}})^{\mathrm{T}} \\ \boldsymbol{0} & \boldsymbol{\Phi}_{q^{\mathrm{r}}}^{\mathrm{rr}} & \boldsymbol{0} & \boldsymbol{0} \\ \boldsymbol{\Phi}_{q^{\mathrm{e}}}^{\mathrm{er}} & \boldsymbol{\Phi}_{q^{\mathrm{r}}}^{\mathrm{er}} & \boldsymbol{0} & \boldsymbol{0} \end{bmatrix} \begin{bmatrix} \Delta \boldsymbol{q}^{\mathrm{ee}} \\ \Delta \boldsymbol{q}^{\mathrm{rr}} \\ \Delta \lambda^{\mathrm{rr}} \\ \Delta \lambda^{\mathrm{er}} \end{bmatrix} = - \begin{bmatrix} \boldsymbol{F}^{\mathrm{e}} \\ \boldsymbol{F}^{\mathrm{r}} \\ \boldsymbol{\Phi}^{\mathrm{rr}} \\ \boldsymbol{\Phi}^{\mathrm{er}} \end{bmatrix} \tag{8}$$

where $\boldsymbol{B}$ is the transformation matrix with the relationship between Cartesian and relative coordinates, $\boldsymbol{q}$ is the relative generalized coordinate, $\boldsymbol{M}$ is the mass matrix, $\ddot{\boldsymbol{r}}$ is the Cartesian acceleration, $\boldsymbol{\Phi}$ is the constraint equation, $\boldsymbol{\lambda}$ is the Lagrange multiplier, $\boldsymbol{Q}$ and $\boldsymbol{F}$ are the force vectors, the superscript "r" means the quantity for the rigid body, the superscript "rr" means the quantities between rigid bodies, the superscript "e" means the quantities for the flexible nodal body, the superscript "er" means the quantities between a flexible nodal body and a rigid body and the superscript "ee" means the quantities between flexible nodal bodies.

According to the MFBD system equation of the launching system, the dynamic equation puts the finite element and multi-body system into one solver to get the solution and realizes the complete coupling calculation of the finite element flexible body and multi-body dynamics.[15] With the MFBD technology, the collision and non-linear deformation between flexible bodies can be sophisticatedly considered in the simulation process, and some information such as dynamic stress and dynamic strain of structure components can be obtained directly.[15,19–21]

4. Model verification

To accurately predict the rotating missile's LPAV, the built dynamics prototype model of the spiral guideway launching system must be verified. The verification methods can be sorted as subjective confirmation, dynamic interrelation and frequency spectrum analysis, etc.[25] Subjective confirmation and dynamic interrelation method are qualitative and their verification accuracy is relatively low. Spectrum analysis is quantitative, which confirms the validity of the simulation model by comparing the simulation model output spectrum with the experimental system test spectrum; therefore, it is applicable to the validation of dynamic performance of the virtual prototype model.

Because of the dynamic characteristics of the prototype model of the rotating missile launching system, the frequency spectrum analysis is adopted for verification. The verification process with spectrum analysis is: based on the analysis of the related parameter sensitivity, the model parameters are adjusted to enable the frequency spectrum chart of the pitching vibration angular velocity of the launching canister orifice consistent in both the virtual test and the physical test.

Because of the complexity and randomness of the missile launching process, the pitching vibration angular velocity of the launching canister orifice measured by the test has a certain difference in the time domain, but very small difference in the frequency domain. Several test results proved that: the spectrum structure of the many times measuring pitching vibration angular velocity of launching canister orifice are basically identical, so this paper only gives the spectrum analysis of one test among them as a representative.

Fig. 3 shows the contrast curves of power spectrum density (PSD) of the pitching vibration angular velocity of the launching canister orifice in both virtual test and physical test at 20° launching angle, with 13 kN average thrust and 6400 Hz sampling frequency. Fig. 3 indicates that through multi-adjustment of the model parameter, the consistency of the results obtained in the virtual test and physical test is quite good, which effectively proves the veracity of the built prototype model.

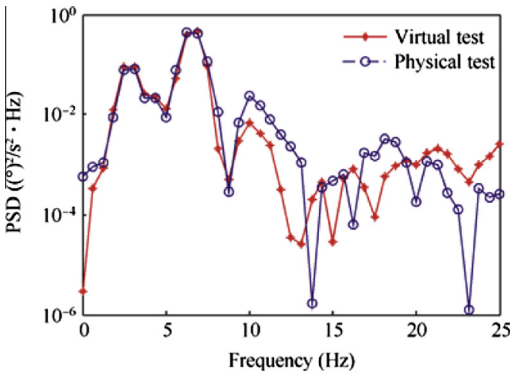

Fig. 3 Contrast of PSD of pitching vibration angular velocity.

5. Virtual tests and result analysis

When this verified prototype model is under different conditions, with MFBD technology the research can be conducted on the influence of a series of factors on LPAV, such as launching angle, clearance between missile and canister, thrust change, thrust eccentricity and mass eccentricity, etc.

5.1. Influence of launching angle on LPAV

When the clearance value is 0.4 mm, the average thrust is 13000 N, the launching angle range is 0°–60°; thrust eccentricity and mass eccentricity is not considered, the simulation results are shown in Figs. 4 and 5. From the two figures we can see that the launching angle has a significant influence on LPAV; the bigger the launching angle is, the lower LPAV will be. Within the launching angle range of 0°–60°, LPAV scattering range is about 12.5°/s; Within the launching angle range of 0°–20°, there is tiny influence on LPAV; within the launching angle range of 20°–60°, there is a significant influence on LPAV.

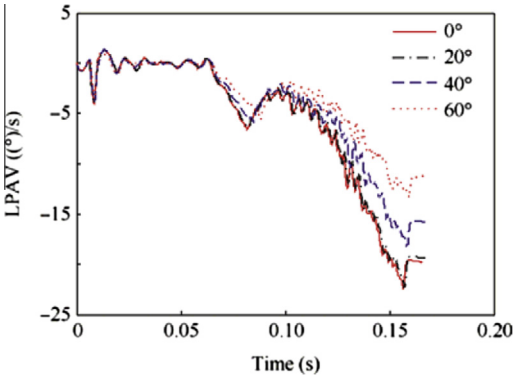

Fig. 4 LPAV vs time for different launching angles.

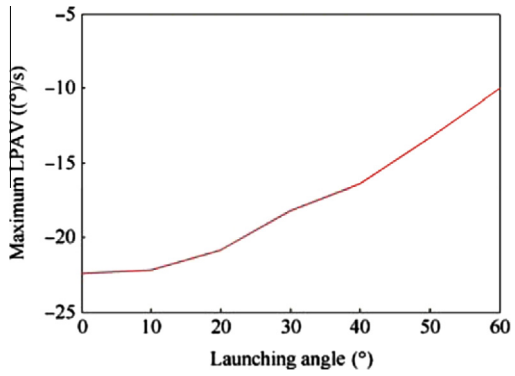

Fig. 5 Maximum LPAV vs launching angles.

5.2. Influence of clearance between launching canister and missile on LPAV

When the launching angle is 20°, the average thrust is 13000 N, the thrust and mass eccentricities are not considered and the clearance range is 0.2–0.8 mm, the simulation results are shown in Figs. 6 and 7. From the two figures we find that the clearance has some influences on LPAV; within the clearance range of 0.2–0.8 mm, LPAV scattering range is about 2°/s; at the clearance value of 0.4 mm, LPAV is the lowest and is about −20.7°/s.

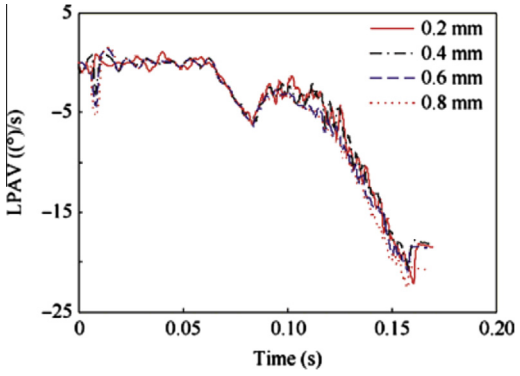

Fig. 6 LPAV vs time for different clearances between launching canister and missile.

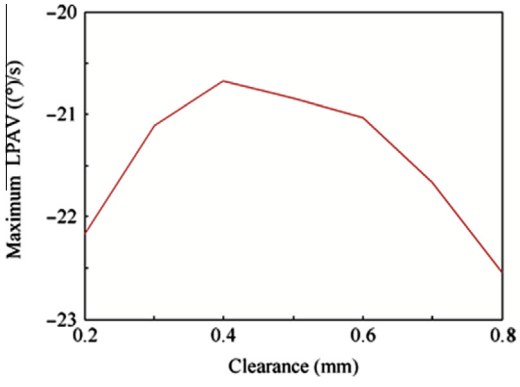

Fig. 7 Maximum LPAV vs clearances between launching canister and missile.

5.3. Influence of thrust change on LPAV

When the launching angle is 20°, the clearance value is 0.4 mm, the thrust and mass eccentricity is not considered and the thrust range is 11.4–15.0 kN, the simulation results are shown in Figs. 8 and 9. The two figures indicate that the engine thrust has some influences on LPAV; the bigger thrust is, the lower LPAV will be. Within allowed thrust change range, LPAV scattering range is about 2.5°/s.

5.4. Influence of thrust eccentricity on LPAV

When the launching angle is 20°, the clearance value is 0.4 mm, the average thrust is 13 kN, the mass eccentricity is not considered and the thrust eccentricity is 3′, the research is conducted the influence of different thrust eccentricity direction on LPAV. Fig. 10 shows the simulation results. Thrust eccentricities 1–2 represent the different directions of thrust eccentricity. When the thrust eccentricity is 3′, the influence on LPAV is the smallest and can even be ignored.

5.5. Influence of mass eccentricity on LPAV

When the launching angle is 20°, the average thrust is 13 kN, the clearance value is 0.4 mm, the thrust eccentricity is not considered and the mass eccentricity is 0.54 mm, the research is conducted on the influence of different mass eccentricity on LPAV. The simulation results are shown in Fig. 11, mass eccentricities 1–2 represent the different positions of mass eccentricity. The figure indicates that LPAV changes per

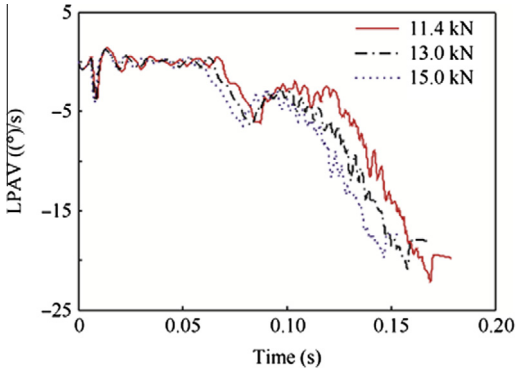

Fig. 8 LPAV vs time for different thrusts.

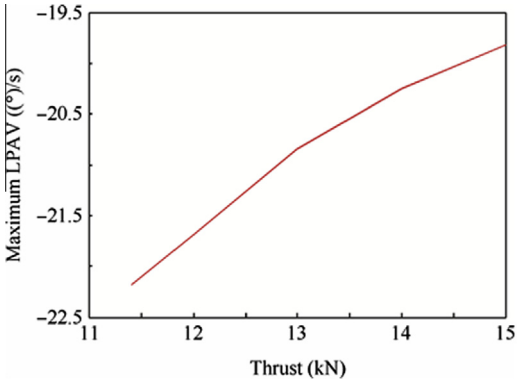

Fig. 9 Maximum LPAV vs thrust.

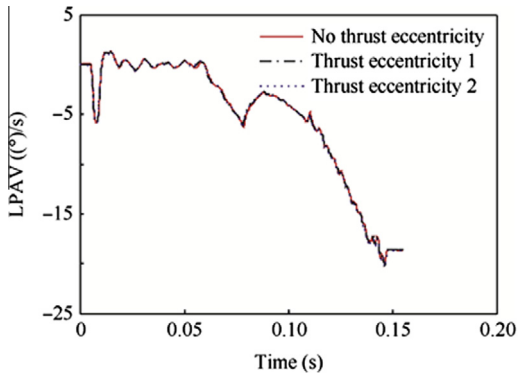

Fig. 10 LPAV vs time for different thrust eccentricities.

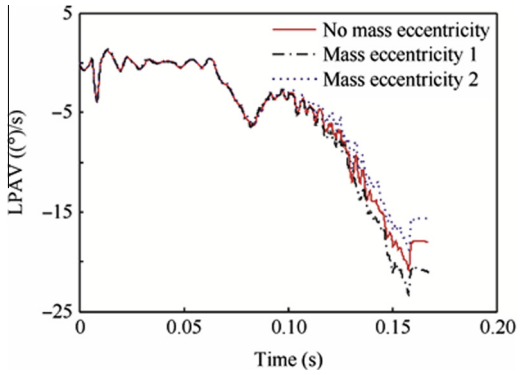

Fig. 11 LPAV vs time for different mass eccentricities.

different mass eccentricity position. When the mass eccentricity is 0.54 mm, LPAV scattering range is about 2.5°/s.

5.6. Influence of multifactor combination on LPAV

The influence of single factor on LPAV is analyzed in the previous paragraphs; however, all kinds of interference factors are very complex. Therefore, it is quite necessary to have a combination analysis on the factors.

According to the data offered by overall designer, multiple situations of these influence factors can be gained. Table 4 shows only 12 ones of these situations. According to the defined parameter in Table 4, simulation results are shown

Table 4 Multifactor combination.

Case	Launching angle (°)	Clearance (mm)	Thrust (kN)	Mass eccentricity (mm)	Thrust eccentricity (′)
1	20	0.2	11.4	0.1	3
2	20	0.2	15.0	0.9	3
3	20	0.8	11.4	0.1	3
4	20	0.8	15.0	0.9	3
5	40	0.2	11.4	0.1	3
6	40	0.2	15.0	0.9	3
7	40	0.8	11.4	0.1	3
8	40	0.8	15.0	0.9	3
9	60	0.2	11.4	0.1	3
10	60	0.2	15.0	0.9	3
11	60	0.8	11.4	0.1	3
12	60	0.8	15.0	0.9	3

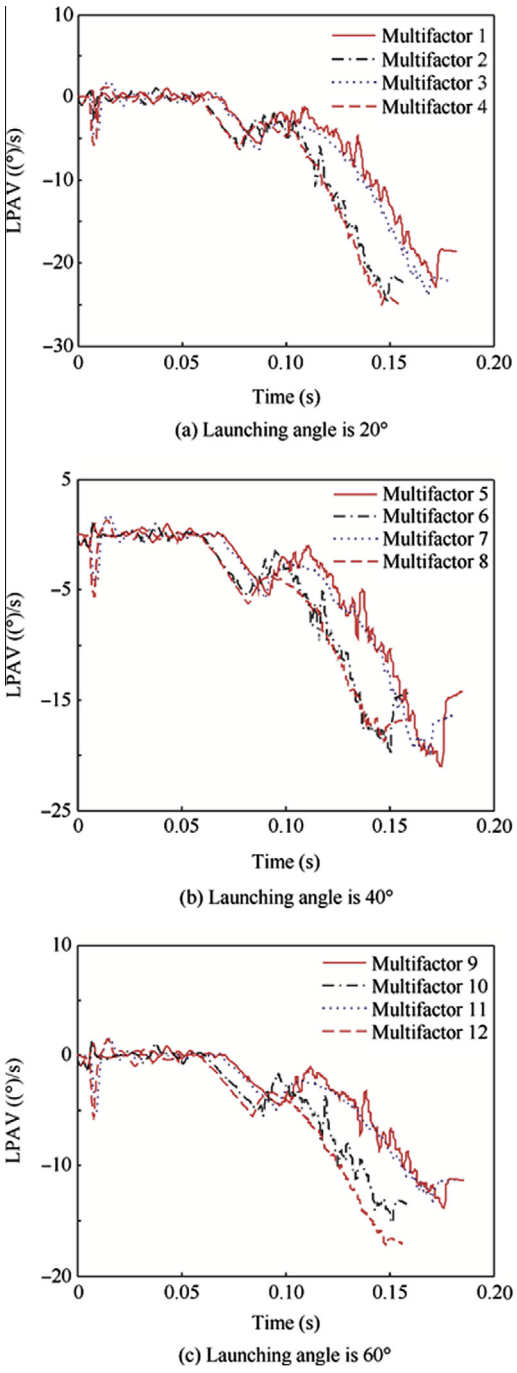

Fig. 12 LPAV vs time for multifactor combination.

in Fig. 12, which indicate that LPAV scattering range is about 6°/s with the multi-factor combination; when the launching angle is 20°, LPAV range is about (22 ± 3)°/s; when the launching angle is 40°, LPAV range is about (18 ± 3)°/s; when the launching angle is 20°, LPAV range is about (14 ± 3)°/s.

6. Changing law of LPAV

The virtual test simulation results reveal that among the influences of scattering factors on LPAV, the launching angle is the most significant one. The bigger launching angle is, the lower LPAV will be; the influence of thrust eccentricity is tiny and

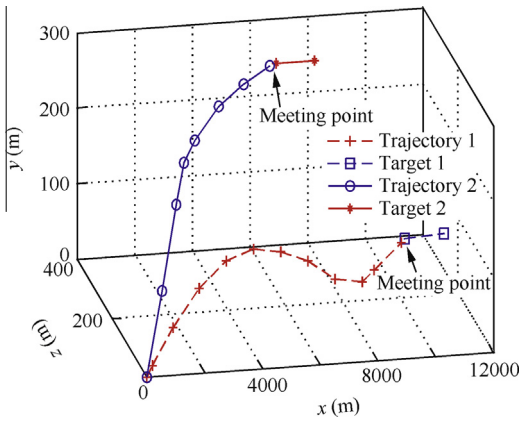

Fig. 13 Flight test validation.

can be ignored. With multifactor combination, at the same launching angle, LPAV's scattering range is about 6°/s, indicating a deviation of ±3°/s.

The virtual test data from the simulation can be fitted with the linear regression method to obtain the changing law of LPAV; its corrected and simplified mathematics model can be expressed as[26]

$$\dot{\theta}_{\mathrm{p}} = \begin{cases} (0.15\varphi - 25) \pm 3, & 0^{\circ} < \varphi \leqslant 20^{\circ} \\ (0.2\varphi - 26) \pm 3, & 20^{\circ} < \varphi \leqslant 60^{\circ} \end{cases} \tag{9}$$

where $\dot{\theta}_{\mathrm{p}}$ is LPAV, and φ is the launching angle. LPAV offered by this corrected model enables better consistent between the multiple theoretic ballistic trajectory and flight test optical measuring ballistic trajectory. So this model is quite applicable. Fig. 13 shows two flight trajectories of the closed-loop test.

7. Conclusions

(1) MFBD technology can truly simulate the contact nonlinearity and material nonlinearity of complex objects and be able to accurately and quickly calculate the contact force between the flexible bodies and flexible body and rigid body, as well as non-linear deformation.

(2) Among the influences of scattering factors on LPAV, the launching angle is the most one. The bigger the launching angle is, the lower LPAV will be; the influence of thrust eccentricity is tiny and can be ignored. With combined influence such as the clearance between missile and canister, mass eccentricity and thrust change etc., at the same launching angle, LPAV's scattering range is about 6°/s.

(3) Using the linear regression method, a simplified mathematics model of corrected changing law of LPAV is obtained, which provides more accurate input for exterior trajectory optimization design and is verified by physical flight tests. The research result has important engineering significance for tactical missile's development.

Acknowledgements

The authors are grateful to the anonymous reviewers for their critical and constructive review of the manuscript. This study was supported by the Key Special Funds for National Defense Basic Scientific Research of China (No. C0320110005).

References

1. Qian XF, Lin RX, Zhao YN. *Missile flight mechanics*. 1st ed. Beijing: Beijing Institute of Technology Press; 2000. p. 136–43 [Chinese].
2. Bi SH, Li HB, Li LH, Fang YQ. Active control of initial disturbance of rockets and missile. *J B Inst Technol* 2001;**10**(2):143–8.
3. Pamadi BN, Neirynck TA, Hotchko NJ, Tartabini PV, Scallion WI, Murphy KJ, et al. Simulation and analysis of stage separation of two-stage reusable launch vehicles; 2005. Report No.: AIAA-2005-3247.
4. Liao SS, Wu C. Launching dynamics modeling of guided aircraft missile and virtual prototype simulation. *Trans B Inst Technol* 2011;**31**(9):1013–7 [Chinese].
5. Cochran JE, Beaty JR. Simulation of the flight of a short range air defense system rocket before radar acquisition. Auburn (AL): Mechanical Engineering Department, School of Engineering, Auburn University; 1977. Report No.: ADA042036.
6. Cochran JE, Christensen DE. Launcher_rocket dynamics and passive control; 1981. Report No.: AIAA-1981-1902.
7. Yao CR, Tang GL. *Rocket and missile launching dynamics*. 1st ed. Beijing: Beijing Institute of Technology Press; 1996 [Chinese].
8. Bittle DA. TACAW/SFMTI launcher simulation. Alabama (CA): Structures Directorate Research, Development, and Engineering Center; 1997. Report No.: RD-ST-92-2.
9. Liu G, Lv JX. Dynamics simulation of rifle launching of certain missile by means of virtual prototype technology. *Tactical Missile Technol* 2005(5);61–5 [Chinese].
10. Cochran JE, No TS, Foster WA. Dynamics of flexible missile/launcher systems; 1992. Report No.: AIAA-1992-4492-CP.
11. Cochran JE, Cheng YM, Bigelow S, Sandidge D, Benner J. Multiple body missile launcher simulation; 1994. Report No.: AIAA-1994-3451-CP.
12. Fu DB, Jiang Y. Dynamics simulation of guided missile launcher based on coupled rigid and flexible model. *J Syst Simul* 2009;**21**(6):1789–91 [Chinese].
13. Gao XD, Bi SH, Chen Z. Flexible multi-body dynamics analysis during missile launching based on improved Craig-Bampton method. *J Solid Rocket Technol* 2011;**34**(5):559–63 [Chinese].
14. Baldesi G, Toso M. European Space Agency's launcher multibody dynamics simulator used for system and subsystem level analyses. *CEAS Space J* 2012;**3**(1–2):27–48.
15. Jiao XJ, Zhang JW, Peng BB. *RecurDyn multi-body system optimization and simulation technology*. Beijing: Tsinghua Publishing House; 2010 [Chinese].
16. Wijker J. *Spacecraft structure*. Heidelberg: Springer; 2008, p. 281–98.
17. Lee D, Hodges DH, Patil MJ. Multi-flexible-body dynamic analysis of horizontal axis wind turbines. *Wind Energ* 2002;**5**(4):281–300.
18. Lee D, Hodges DH. Multi-flexible-body analysis for application to wind turbine control design. Atlanta (GA): Georgia Tech Research Corporation; 2004. Report No.: NREL/SR-500-35228.
19. Türtscher A, Faβbender F, Kelichhaus T. Simulation of dynamic stresses including flexible contact s using MFBD technology. SAE; 2006. Report No.: 2006-01-2886.
20. Zaeh M, Siedl D. A new method for simulation of machining performance by integrating finite element and multi-body simulation for machine tools. *Ann CIRP* 2007;**56**(1):383–6.
21. Liu Y, Chen GD, Li JS, Xue YJ. Flexible multibody simulation approach in the analysis of friction winder. *Adv Mater Res* 2010;**97–101**:2594–7.
22. Yao CR, Zhang B. *The design of the launching device for rocket and missile*. 1st ed. Beijing: Beijing Institute of Technology Press; 1998 [Chinese].

23. Li WL. A new method for structural model updating and joint stiffness identification. *Mech Syst Signal Process* 2002;**16**(1):155–67.
24. Mao KM, Li B, Wu J, Shao XY. Stiffness influential factors-based dynamic modeling and its parameter identification method of fixed joints in machine tools. *Int J Mach Tools Manuf* 2010;**50**(2):156–64.
25. Wu DL, Ma JS, Li W. Verification validation and certification based on virtual prototype simulation system. *Comput Simul* 2006;**23**(7):69–72 [Chinese].
26. Weisberg S. *Applied linear regression*. 3rd ed. New Jersey: John Wiley & Sons, Inc.; 2005. p. 21–7.

Liu Guang is a Ph.D. candidate at Department of Mechanical and Engineering Science, Fudan University, and a senior engineer at Shanghai Electro-Mechanical Engineering Institute, China. His research interests are mechanical system dynamics and aircraft design.

Xu Bin is a Ph.D. candidate at Department of Mechanical and Engineering Science, Fudan University, and a senior engineer at Shanghai Electro-Mechanical Engineering Institute, China. His research interests are nonlinear dynamics and aircraft design.

Jiao Xiaojuan is a Ph.D. candidate at Department of Mechanical and Engineering Science, Fudan University, China. Her research interests are in the areas of multi-body system dynamics.

Zheng Tiesheng is a professor and doctoral supervisor at Department of Mechanical and Engineering Science, Fudan University, China. His research fields are mechanical system dynamics, fluid-structure coupling vibration, nonlinear dynamics, rotor dynamics and computational mechanics.